Free-carrier absorption in asymmetric double quantum well structures due to static scatterers in the in-plane polarization

C. Ndebeka-Bandou, F. Carosella, R. Ferreira, and G. Bastard
Laboratoire Pierre Aigrain, Ecole Normale Supérieure, CNRS (UMR 8551), Université Pierre et Marie Curie, Université Paris Diderot, 24 rue Lhomond, F-75005 Paris, France
(Received 13 December 2013; published 26 February 2014)

We report on the computation of the free-carrier absorption induced by static scatterers in asymmetric double quantum well structures when the electromagnetic wave propagates along the growth axis. We find that a Drude-like tail exists for this polarization. The absorption is found to be larger than when the wave propagates in the layer plane. Also, intrasubband scattering is found to be more efficient than intersubband scattering. The alloy scattering is found to be particularly efficient.

DOI: 10.1103/PhysRevB.89.075313 PACS number(s): 73.21.Ac, 78.67.Pt

I. INTRODUCTION

One of the possible ways to realize THz sources is the development of quantum cascade lasers (QCLs) [1–3]. However, so far, reports of room temperature operation are still lacking and the search for improvement is intensive [4–6]. The free-carrier absorption (FCA) is a plausible source of losses for far-IR and THz lasers [7–9]. It consists in the reabsoprtion of the laser photons by the free carriers [10], in particular, those that occupy the upper laser subband. FCA arises from intrasubband and intersubband oblique transitions [11] (in the $\vec{k}$ space) activated by static scatterers or phonons. Recently, we proposed a modeling of FCA in QCLs [12], thereby focusing our attention on the standard light polarization for these systems, i.e., electromagnetic waves that propagate in the layer plane with their electric vector parallel to the growth axis. In this paper we examine the FCA in an asymmetric double quantum well structure and we concentrate on the in-plane polarization (propagation parallel to the z growth axis). We shall show that, in stark contrast to what we found when the wave is polarized along z, the FCA exhibits a Drude-like behavior. We shall also demonstrate that FCA can be larger in the in-plane polarization that in the z polarization. Finally, we shall show that the intrasubband FCA is more important than the intersubband one, a feature that again differs from what happens in the z polarization analyzed previously [12]. These features go beyond the specific case of the double quantum well structure and apply as well to single or multiple quantum wells but not to superlattices displaying a significant electronic dispersion for the motion along the growth axis.

In the following, we concentrate on the optical intra- and intersubband transitions mediated by static scatterers such as interface defects, Coulombic donors, and alloy disorder, and we show that the dependence of the FCA upon the photon energy is significantly modified by the polarization of the electromagnetic wave. Along the same line, we compare the different FCA magnitudes for two different polarization configurations in a two-dimensional heterostructure. Notice that with an in-plane light polarization, the electromagnetic wave propagates through an inhomogeneous medium and thus an absorption coefficient cannot be defined as it is usually done for bulk materials or QCLs with standard light polarization. For that reason we shall evaluate the energy loss rate associated with intra- and intersubband oblique transitions and not express it in terms of the absorption coefficient.

II. MODEL

We consider an asymmetric 26/3.1/12.6 nm double quantum well (DQW) where the wide well is located on the left hand side of the structure. The conduction band offset is set to $V_b = 360$ meV corresponding to the $In_{0.53}Ga_{0.47}As/GaAs_{0.51}Sb_{0.49}$ ternary system [13]. The carrier effective masses are $m^* = 0.045m_0$ in the barrier material and $0.043m_0$ in the well material, respectively. The DQW contains few carriers with an electronic sheet density equal to $n_e = 2.17 \times 10^{10}$ cm^{-2}. This structure supports nine bound states E_n for the z motion, where n is the subband index. In the absence of disorder and if nonparabolicity is neglected, the two-dimensional eigenstates of the ideal DQW can be written as

$$\langle \vec{\rho}, z | n, \vec{k} \rangle = \chi_n(z) \frac{1}{\sqrt{S}} e^{i\vec{k}\cdot\vec{\rho}}, \tag{1}$$

$$\varepsilon_{n\vec{k}} = E_n + \frac{\hbar^2 k^2}{2m^*}, \tag{2}$$

where $\vec{\rho} = (x, y)$ is the in-plane position, $\vec{k}$ the two-dimensional wave vector, and $S = 200 \times 200$ nm^2 the sample area.

In the presence of static scatterers, the corresponding envelope function Hamiltonian is

$$H = \frac{p^2}{2m^*} + V_b(z) + V_{\rm dis}(\vec{\rho}, z), \tag{3}$$

where $V_{\rm dis}(\vec{\rho}, z)$ is the electron potential due to either interface roughness, Coulombic donors, or alloy disorder.

Figure 1 shows the conduction band profile of the DQW structure and the squared modulus of the envelope wave functions χ_2 and χ_3. The interface defects are modeled by Gaussian protrusions of the barrier in the well (repulsive defects) or the well in the barrier (attractive defects) [14]. The Gaussian defects are characterized by their in-plane extension σ and are introduced in the two inner interfaces (labeled z_0; see Fig. 1) of the structure with a fractional coverage of the surface $f = \pi\sigma^2 n_{\rm def}$, where $n_{\rm att}$, $n_{\rm rep}$, and $n_{\rm def} = n_{\rm att} + n_{\rm rep}$ are, respectively, the areal concentrations

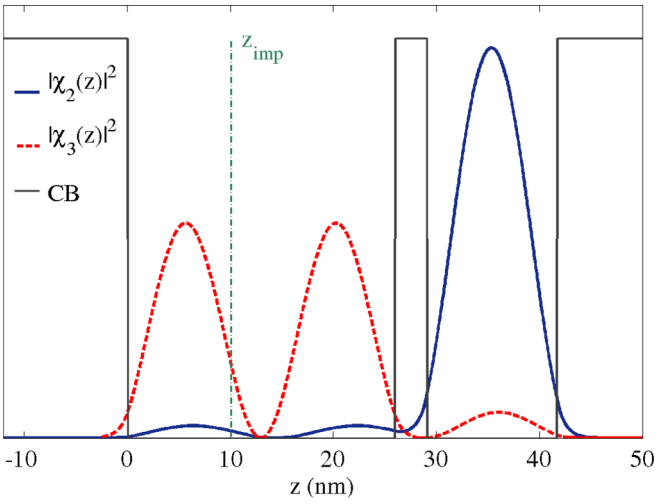

FIG. 1. (Color online) Conduction band profile for the 26/3.1/12.6 nm DQW and squared modulus of the χ_2 (blue solid line) and χ_3 (red dashed line) envelope wave functions. The vertical green dashed-dotted line represents the donors plane at the position $z_{\rm imp} = 10$ nm. The interface defects are located in the two inner interfaces of the structure, i.e., at $z_0 = \{26\ {\rm nm}, 29.1\ {\rm nm}\}$.

of attractive defects ($n_{\rm att}$), repulsive defects ($n_{\rm rep}$), and their sum ($n_{\rm def}$). The Coulombic donors sit on a single doping plane located at $z_{\rm imp} = 10$ nm from the left hand side of the wide well (see Fig. 1) with an areal concentration equal to n_e corresponding to a distribution of eight impurities on the Oxy plane. The strength of Coulombic scattering depends upon the impurity location. Putting the impurities near the maximum (minimum) of the envelope function product of the initial and final subbands would produce a larger (smaller) FCA than is produced with $z_{\rm imp} = 10$ nm. Recently, we analyzed this dopant engineering of the intersubband linewidth and line shape in multiwell heterostructures [15]. Using the virtual crystal approximation (VCA) [16], we define the alloy disorder potential as a delta potential characterized by its effective strength ΔV and the volume of the VCA unit cell Ω_0.

In the following, we study the optical intra- and intersubband transitions mediated by the static disorder of the structure. If the electric field of the electromagnetic wave is polarized in the layer Ox (Oy), the light-matter coupling is described by the dipolar matrix element $\langle f|p_\perp|i\rangle$, where $p_\perp = p_x$ (p_y). Thus, for an electromagnetic wave with an angular frequency ω, the energy loss rate associated with the disorder-assisted transitions $|n\vec{k}\rangle \rightarrow |m\vec{k'}\rangle$ is given by

$$P_{nm}(\omega) = \frac{\pi e^2 F_{\rm las}^2}{m^{*2}\omega} \sum_{\vec{k},\vec{k'}} (f_{n\vec{k}} - f_{m\vec{k'}}) |\langle \Psi_{m\vec{k'}}|p_\perp|\Psi_{n\vec{k}}\rangle|^2 \times \delta(\varepsilon_{m\vec{k'}} - \varepsilon_{n\vec{k}} - \hbar\omega), \quad (4)$$

where $F_{\rm las}$ is the intensity of the laser field, $\Psi_{n\vec{k}}$ and $\Psi_{m\vec{k'}}$ are the perturbed wave functions for the initial and final states, respectively, and $f_{n\vec{k}}$ and $f_{m\vec{k'}}$ are their respective occupation functions. On account of the low carrier concentration and the relatively large electron temperature ($T = 100$ K), we assume a thermalized distribution inside the initial E_n subband and take the occupation functions as Boltzmann distributions.

The perturbed wave functions $\Psi_{n\vec{k}}$ and $\Psi_{m\vec{k'}}$ are evaluated by expanding the electronic states to first order in $V_{\rm dis}$, following the perturbative approach of Ref. [12]. Then the dipolar matrix element of Eq. (4) reduces to

$$|\langle \Psi_{m\vec{k'}}|p_\perp|\Psi_{n\vec{k}}\rangle|^2 = \frac{|\langle m\vec{k'}|V_{\rm dis}|n\vec{k}\rangle|^2}{\omega^2}(k_\perp - k'_\perp)^2, \quad (5)$$

where $k_\perp = k_x(ky)$. By averaging over the positions of the interface defects and donors, the squared modulus of Eq. (5) becomes proportional to the number of defects and donors and for the interface defects, Coulombic donors, and alloy disorder, respectively, the analytical development of Eq. (4) gives

$$P_{nm}^{\rm def}(\omega) = \frac{\pi e^2 F_{\rm las}^2 \sigma^4 V_b^2}{\omega^3 \hbar^2 m^*} n_e (1 - e^{-\beta\hbar\omega}) \times \Lambda_{nm}^{\rm def} \int_0^{2\pi} d\theta \int_0^\infty du e^{-u} e^{-\sigma^2 q_{nm}^2(u)} q_{nm}^2(u), \quad (6)$$

$$P_{nm}^{\rm imp}(\omega) = \frac{e^6 F_{\rm las}^2 n_{\rm imp}}{16\omega^3\hbar^2 m^* (\varepsilon_0\varepsilon_r)^2} n_e (1 - e^{-\beta\hbar\omega}) \times \int_0^{2\pi} d\theta \int_0^\infty du e^{-u} \left|\Lambda_{nm}^{\rm imp}[q_{nm}(u)]\right|^2, \quad (7)$$

$$P_{nm}^{\rm alloy}(\omega) = \frac{e^2 F_{\rm las}^2 x(1-x)\Delta V^2 \Omega_0}{\omega^3\hbar^2 m^*} n_e (1 - e^{-\beta\hbar\omega}) \times \Lambda_{nm}^{\rm alloy} \int_0^{2\pi} d\theta \int_0^\infty du e^{-u} q_{nm}^2(u), \quad (8)$$

with

$$q_{nm}(u) = \frac{2m^*}{\beta\hbar^2}[2u + \beta(\hbar\omega - E_{nm}) \times -2\sqrt{u}\sqrt{u + \beta(\hbar\omega - E_{nm})}\cos\theta], \quad (9)$$

$$\Lambda_{nm}^{\rm def} = \sum_{z_0} \left(n_{\rm att} \left| \int_{z_0-h}^{z_0} dz \chi_n(z)\chi_m(z) \right|^2 + n_{\rm rep} \left| \int_{z_0}^{z_0+h} dz \chi_n(z)\chi_m(z) \right|^2 \right), \quad (10)$$

$$\Lambda_{nm}^{\rm imp}(q_{nm}(u)) = \int dz \chi_n(z)\chi_m(z) e^{-q_{nm}(u)|z - z_{\rm imp}|}, \quad (11)$$

$$\Lambda_{nm}^{\rm alloy} = \int_{\rm alloy} dz \chi_n(z)^2 \chi_m(z)^2, \quad (12)$$

and where $u = \frac{\beta\hbar^2 k^2}{2m^*}$, $\beta = (k_B T)^{-1}$, ε_r is the relative dielectric constant, and $E_{nm} = E_m - E_n$ is the bare transition energy.

III. RESULTS AND DISCUSSION

We have numerically evaluated the contributions to the energy loss rate by computing Eqs. (6)–(8) for the DQW structure described above and for $n = 2$ and $m = 2$ (intrasubband transition) or $m = 3$ (intersubband transition). The fractional coverage of interface defects was set to $f = 0.3$ and the defect size to $\sigma = 5.6$ nm. Since the electronic wave functions are mostly localized in the wells of the structure (see Fig. 1),

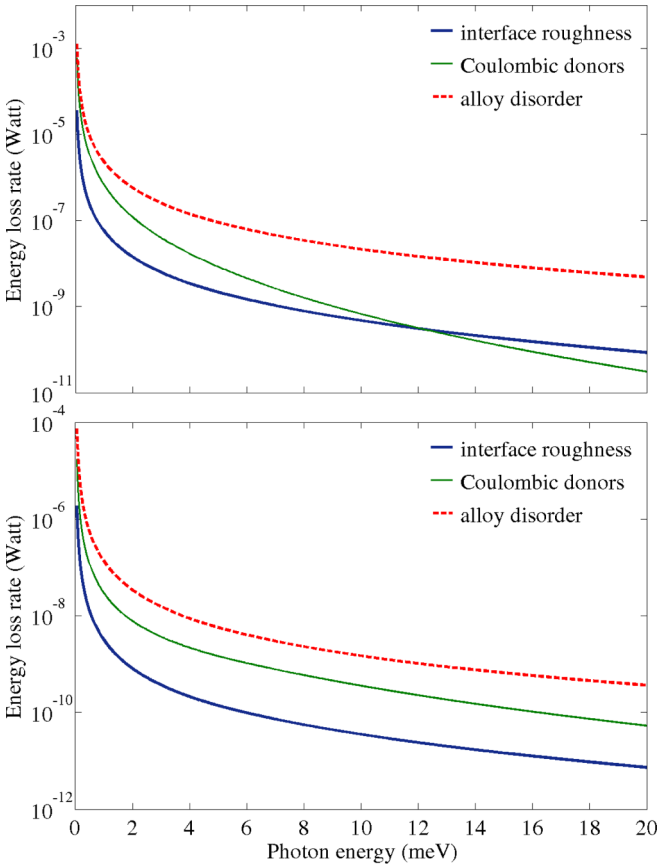

FIG. 2. (Color online) Energy loss rate P_{nm} vs the photon energy $\hbar\omega$ for the intrasubband E_2 (upper panel) and intersubband $E_2 - E_3$ (lower panel) transitions. P_{nm} is calculated by taking into account either the interface roughness (blue solid line), donors (green solid line), or alloy disorder (red dashed line). The electromagnetic wave is polarized in the layer plane. $T = 100$ K.

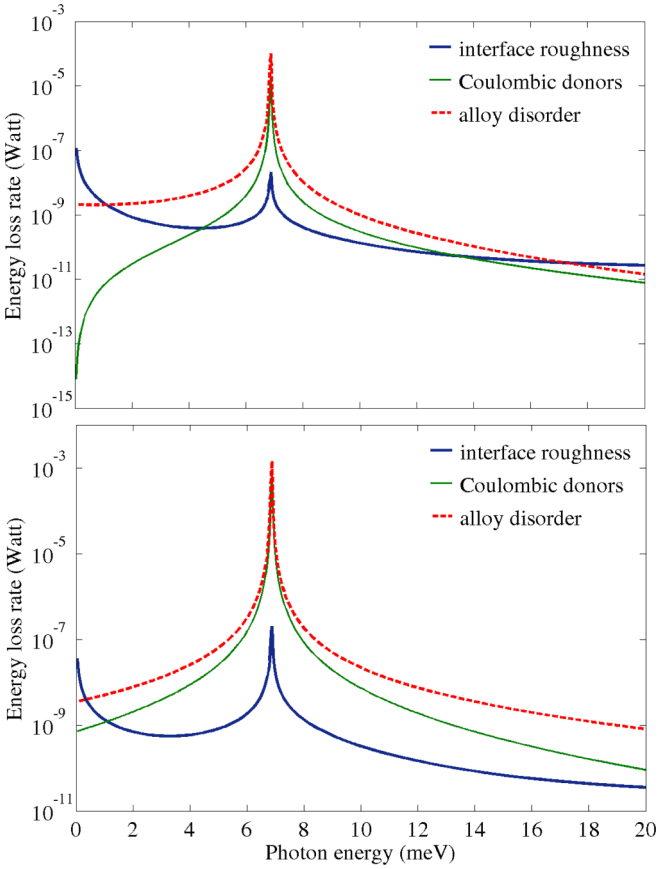

FIG. 3. (Color online) Energy loss rate P_{nm} vs the photon energy $\hbar\omega$ for the intrasubband E_2 (upper panel) and intersubband $E_2 - E_3$ (lower panel) transitions. P_{nm} is calculated by taking into account either the interface roughness (blue solid line), donors (green solid line), or alloy disorder (red dashed line). The electromagnetic wave is polarized along the growth axis. $E_3 - E_2 = 6.8$ meV. $T = 100$ K.

we considered the alloy disorder in the GaInAs wells only, with an alloy fraction of $x = 0.53$ and an effective strength of $\Delta V = 0.6$ eV [17]. Here, $F_{\rm las} = 1$ kV cm^{-1}.

We show in Fig. 2 the energy loss rate versus the photon energy $\hbar\omega$. We compare the situation where either the interface defects, the Coulombic donors, or the alloy disorder are the scatterers and where the electromagnetic wave is polarized along an in-plane direction. As expected from Eqs. (6)–(8), the plots of Fig. 2 display a dependence of the energy loss rate upon the photon energy that goes as ω^{-p}, where $p > 0$ and depends on the type of scatterer. In this configuration, the conduction states are extended in the x and y directions, and the carrier free motion then occurs in the same plane as the electric field direction. Thus, the absorption processes can be reliably estimated by the semiclassical description, assuming that the carriers are accelerated by the electric force $-e\vec{F}_{\rm las}$. As a consequence, the ω^{-p} ($p \sim 2$–3) bulk behavior, which is characteristic of the Drude-like approach [18,19], is recovered in this two-dimensional system for this in-plane polarization configuration.

We also note that the intensity of the intrasubband energy loss rate is of one order of magnitude larger than the intersubband corresponding one. This can be readily explained by the larger wave-function overlap in the factor Λ_{nm} of Eqs. (6)–(8) for the intrasubband events, or, stated differently, by the fact that the intersubband dipolar matrix element $\langle n\vec{k}|p_\perp|m\vec{k}'\rangle = \delta_{n,m}\delta_{\vec{k},\vec{k}'}\hbar k_\perp$ leads to intersubband oblique transitions that are forbidden by both wave-vector and energy conservation in an ideal system, while the intrasubband transitions are forbidden only by wave-vector conservation. For comparison, we computed the energy loss rate in the z-polarization configuration, following the quantum mechanical treatment of FCA established in Ref. [12]. The results are shown in Fig. 3 for the two types of transitions and for the same material and disorder parameters used in Fig. 2. Instead of a divergence at $\omega \to 0$, the plots of Fig. 3 display a strong increase when $\hbar\omega$ approaches the bare transition energy $E_3 - E_2$. This feature is due to the virtual intermediate coupling in subband E_3 that is necessary to get a nonzero absorption for these oblique transitions, as explained in Ref. [12]. By comparing the intra- and intersubband contributions, we get the reverse trend from that in the in-plane case: For a given scattering source and in the z-polarization case, the intrasubband process displays a weaker energy loss rate than the intersubband one. This contrast is due to the different dipolar matrix elements entering the energy loss rate

calculation in the z polarization: $\langle n\vec{k}|p_z|m\vec{k}'\rangle = \langle n|p_z|m\rangle\delta_{\vec{k},\vec{k}'}$ leads to intrasubband transitions that are forbidden by both energy and wave-vector conservation in an ideal system, and to oblique intersubband transitions that are only forbidden by wave-vector conservation [12]. This feature also explains that, far from the resonance, the intrasubband energy loss rate for the z polarization is at least two orders of magnitude weaker than the corresponding one in the in-plane configuration, while the intersubband events lead to a similar energy loss rate magnitude for both polarizations.

Finally, Figs. 2 and 3 show that FCA is a more efficient loss mechanism when the elastic scattering is dominated by the alloy disorder contribution in ternary two-dimensional heterostructures. Notice that the alloy disorder has already been demonstrated as being an efficient scattering mechanism in this kind of material [20], characterized by an indium concentration ($x = 0.53$) that is close to the one ($x = 0.5$) that maximizes the alloy scattering efficiency.

IV. CONCLUSION

We have evaluated FCA in asymmetric DQW structures associated with static scatterers when the electromagnetic wave propagates along the growth axis. For such a polarization no absorption coefficient can be defined. The computation of the energy loss rate allows, for a given intensity of the electromagnetic field, to compare the absorption for the in-plane polarization to the one for the polarization along the growth axis. We found that the electromagnetic waves that propagate along the growth axis are more absorbed than those that propagate in the layer plane and that their absorption can be described in terms of a Drude-like decrease, $P(\omega) \approx \omega^{-p}$, where p is positive and depends on the nature of the scattering mechanism. This result contrasts strikingly with the case of QCL losses due to FCA. Moreover, when the electromagnetic wave is in-plane polarized, the intrasubband absorption is found to be significantly larger than that associated with oblique intersubband transitions, because these have a reduced amplitude compared with the intersubband transitions. This result is the opposite of the one evaluated for the standard QCL polarization.

ACKNOWLEDGMENTS

G.B. thanks the Technical University Vienna for hospitality. Discussions with A. Wacker, G. Strasser, and K. Unterrainer are gratefully acknowledged.

[1] J. Faist, F. Capasso, D. L. Sivco, C. Sirtori, A. L. Hutchinson, and A. Y. Cho, Science **264**, 553 (1994).
[2] C. Gmachl, F. Capasso, D. L. Sivco, and A. Y. Cho, Rep. Prog. Phys. **64**, 1533 (2001).
[3] R. Köhler, A. Tredicucci, F. Beltram, H. Beere, E. Linfield, G. Davies, D. Ritchie, R. C. Iotti, and F. Rossi, Nat. Photonics **417**, 156 (2002).
[4] C. Walther, M. Fischer, G. Scalari, R. Terazzi, N. Hoyler, and J. Faist, Appl. Phys. Lett. **91**, 131122 (2007).
[5] B. S. Williams, Nat. Photonics **1**, 517 (2007).
[6] S. Kumar, C. W. I. Chan, Q. Hu, and J. L. Reno, Appl. Phys. Lett. **95**, 141110 (2009).
[7] I. Vurgaftman and J. R. Meyer, Phys. Rev. B **60**, 14294 (1999).
[8] J. Faist, Appl. Phys. Lett. **90**, 253512 (2007).
[9] A. Wacker, G. Bastard, F. Carosella, R. Ferreira, and E. Dupont, Phys. Rev. B **84**, 205319 (2011).
[10] W. P. Dumke, Phys. Rev. **124**, 1813 (1961).
[11] C. Ndebeka-Bandou, F. Carosella, R. Ferreira, A. Wacker, and G. Bastard, Appl. Phys. Lett. **101**, 191104 (2012).
[12] F. Carosella, C. Ndebeka-Bandou, R. Ferreira, E. Dupont, K. Unterrainer, G. Strasser, A. Wacker, and G. Bastard, Phys. Rev. B **85**, 085310 (2012).
[13] C. Deutsch, A. Benz, H. Detz, P. Klang, M. Nobile, A. M. Andrews, W. Schrenk, T. Kubis, P. Vogl, G. Strasser, and K. Unterrainer, Appl. Phys. Lett. **97**, 261110 (2010).
[14] F. Carosella, R. Ferreira, G. Strasser, K. Unterrainer, and G. Bastard, Phys. Rev. B **82**, 033307 (2010).
[15] C. Ndebeka-Bandou, A. Wacker, F. Carosella, R. Ferreira, and G. Bastard, Appl. Phys. Express **6**, 094101 (2013).
[16] G. Bastard, *Wave Mechanics Applied to Semiconductor Heterostructures* (EDP Science, Paris, 1996).
[17] J. R. Hayes, A. R. Adams, and P. D. Greene, *GaInAsP Alloy Semiconductors* (Wiley, New York, 1982), p. 189.
[18] N. W. Ashcroft and N. D. Mermin, *Solid State Physics* (Harcourt, New York, 1976).
[19] W. Walukiewicz, L. Lagowski, L. Jastrzebski, M. Lichtensteiger, and H. C. Gatos, J. Appl. Phys. **50**, 899 (1979).
[20] G. Bastard, Appl. Phys. Lett. **43**, 591 (1983).